Comparison of Integrin $\alpha_v\beta_3$ Expression and Glucose Metabolism in Primary and Metastatic Lesions in Cancer Patients: A PET Study Using ^{18}F-Galacto-RGD and ^{18}F-FDG

Ambros J. Beer[1], Sylvie Lorenzen[2], Stephan Metz[3], Ken Herrmann[1], Petra Watzlowik[1], Hans-Jürgen Wester[1], Christian Peschel[2], Florian Lordick[2], and Markus Schwaiger[1]

[1]Department of Nuclear Medicine, Klinikum rechts der Isar, Technische Universität München, Munich, Germany; [2]Department of Hematology and Oncology, Klinikum rechts der Isar, Technische Universität München, Munich, Germany; and [3]Department of Radiology, Klinikum rechts der Isar, Technische Universität München

The expression of $\alpha_v\beta_3$ and glucose metabolism are upregulated in many malignant lesions, and both are known to correlate with an aggressive phenotype. We evaluated whether assessment of $\alpha_v\beta_3$ expression and of glucose metabolism with PET using ^{18}F-galacto-RGD and ^{18}F-FDG provides complementary information in cancer patients. **Methods:** Eighteen patients with primary or metastatic cancer (non–small cell lung cancer [NSCLC], n = 10; renal cell carcinoma, n = 2; rectal cancer, n = 2; others, n = 4) were examined with PET using ^{18}F-galacto-RGD and ^{18}F-FDG. Standardized uptake values (SUVs) were derived by volume-of-interest analysis. ^{18}F-Galacto-RGD and ^{18}F-FDG PET results were compared using linear regression analysis for all lesions (n = 59; NSCLC, n = 39) and for primaries (n = 14) and metastases to bone (n = 11), liver (n = 10), and other organs (n = 24) separately. **Results:** The sensitivity of ^{18}F-galacto-RGD PET compared with clinical staging was 76%. SUVs for ^{18}F-FDG ranged from 1.3 to 23.2 (mean ± SD, 7.6 ± 4.9) and were significantly higher than SUVs for ^{18}F-galacto-RGD (range, 0.3–6.8; mean ± SD, 2.7 ± 1.5; $P < 0.001$). There was no significant correlation between the SUVs for ^{18}F-FDG and ^{18}F-galacto-RGD for all lesions (r = 0.157; P = 0.235) or for primaries, osseous or soft-tissue metastases separately ($P > 0.05$). For the subgroup of lesions in NSCLC, there was a weak correlation between ^{18}F-FDG and ^{18}F-galacto-RGD uptake (r = 0.353; P = 0.028). **Conclusion:** Tracer uptake of ^{18}F-galacto-RGD and ^{18}F-FDG does not correlate closely in malignant lesions. Whereas ^{18}F-FDG PET is more sensitive for tumor staging, ^{18}F-galacto-RGD PET warrants further evaluation for planning and response evaluation of targeted molecular therapies with antiangiogenic or $\alpha_v\beta_3$-targeted drugs.

Key Words: $\alpha_v\beta_3$; ^{18}F-galacto-RGD; ^{18}F-FDG; PET; oncology

J Nucl Med 2008; 49:22–29
DOI: 10.2967/jnumed.107.045864

Received Aug. 1, 2007; revision accepted Oct. 12, 2007.
For correspondence or reprints contact: Ambros J. Beer, MD, Department of Nuclear Medicine, Klinikum rechts der Isar, Technische Universität München, Ismaninger Strasse 22, 81675 Munich, Germany.
E-mail: beer@roe.med.tum.de

Recently, antiangiogenic therapy with drugs such as bevacizumab (Avastin; Roche), a vascular endothelial growth factor (VEGF) antibody, in combination with cytotoxic chemotherapy has proven to be successful in several tumor entities, including metastasized colorectal cancer, breast cancer, and non–small cell lung cancer (NSCLC) (*1*). Moreover, the multitarget tyrosine kinase inhibitors SU11248 (Sutent; Pfizer) and BAY-43-9006 (Nexavar; Bayer HealthCare), both directed against VEGF receptor, have been successfully used as monotherapy in gastrointestinal stroma tumors and metastatic renal cell carcinomas (*2*). Consequently, there is a growing demand for imaging modalities that allow for response assessment and pretherapeutic stratification of patients receiving targeted therapies with antiangiogenic compounds. In this respect, imaging of $\alpha_v\beta_3$ expression is promising for assessment of angiogenesis, as $\alpha_v\beta_3$ is supposed to be a marker of activated, but not resting, vessels (*3*). Moreover, drugs targeting the $\alpha_v\beta_3$ integrin are evaluated in cancer patients in phase 1 and 2 studies (*4,5*). Therefore, we have developed the $\alpha_v\beta_3$-specific tracer ^{18}F-galacto-RGD for PET (*6*). It has been demonstrated that ^{18}F-galacto-RGD PET allows for specific imaging of $\alpha_v\beta_3$ expression and that a significant correlation of $\alpha v\beta 3$ expression and ^{18}F-galacto-RGD uptake exists in tumor xenografts as well as in tumor lesions in cancer patients (*7,8*). However, up to now, it has not been evaluated how ^{18}F-galacto-RGD behaves in comparison with common tracers of tumor metabolism such as ^{18}F-FDG. This is of great importance, as there are reports describing a correlation between angiogenic activity in tumors and ^{18}F-FDG uptake in vitro and in vivo (*9,10*). Moreover, both $\alpha_v\beta_3$ expression and ^{18}F-FDG uptake are believed to correlate with tumor aggressiveness and prognosis in several tumor entities (*11–14*). Therefore, it cannot be excluded that, ultimately, a tracer such as ^{18}F-FDG provides information similar to that of ^{18}F-galacto-RGD, although both tracers have completely

different pharmacodynamic properties. In case of a close correlation between the uptake of these 2 tracers, there would be no need for a specific tracer such as ^{18}F-galacto-RGD, because ^{18}F-FDG is widely available and has been successfully used in clinical routine for years. In this study we compared the tracer uptake of ^{18}F-galacto-RGD and ^{18}F-FDG in primary as well as in metastatic tumor lesions. The goals of this study were to evaluate whether ^{18}F-galacto-RGD and ^{18}F-FDG provide similar or complementary information in cancer patients and to determine the sensitivity of ^{18}F-galacto-RGD for lesion identification.

MATERIALS AND METHODS

Radiopharmaceutical Preparation

Synthesis of the labeling precursor and subsequent ^{18}F labeling were performed as described previously (*15*).

Patients

The study was approved by the ethics committee of the Technische Universität München, and informed written consent was obtained from all patients. Eighteen patients were included in the study (6 female, 12 male; mean age ± SD, 63.8 ± 8.2 y; range, 52–80 y). Inclusion criteria consisted of biopsy-proven metastatic cancer, as determined by clinical staging including contrast-enhanced CT and ^{18}F-FDG PET/CT in all cases and ^{111}In-octreotide scintigraphy in one case (patient 10; Table 1). Further inclusion criteria were age over 18 y, and the absence of pregnancy, lactation period, and impaired renal function (serum creatinine level $>$ 1.2 mg/dL). For further details on the patient population see Table 1.

Contrast-Enhanced CT

CT was performed on 14 patients with a Sensation 64 CT scanner (Siemens Medical Solutions, Inc.) using the following scan parameters: collimation, 64 × 0.6 mm; 120 kV, 200 quality reference mAs (CareDose 4D); 5-mm reconstructed slice thickness/5-mm reconstruction increment; kernel B30 for soft tissues and B60 for the lung. All scans were performed from the thorax to the pelvis, including the head for patients with NSCLC or if brain metastases were clinically suspected. Scans were performed in deep inspiration in the portalvenous phase 70 s after injection of 150 mL of iodine contrast agent by a power injector (Imeron 300; Altana) using a flow of 3 mL/s, followed by a saline bolus (40 mL, 3 mL/s). In 4 patients, contrast-enhanced CT examinations were performed on the Biograph Sensation 16 PET/CT scanner (Siemens) using the following scan parameters: collimation, 16 × 0.75 mm; 120 kV, 150 mAs; 5-mm reconstructed slice thickness/5-mm reconstruction increment; kernel B30 for soft tissues and B60 for the lung. Scans were performed in shallow expiration from the head to the pelvis 70 s after injection of iodine contrast agent (Imeron 300; Altana) with a flow of 3 mL/s, followed by a saline bolus (40 mL; 3 mL/s). An additional low-dose CT scan of the thorax in deep inspiration for analysis of the lungs was performed afterward (120 kV, 50 mAs). All patients received oral contrast agent 1 h before scanning (Megluminioxitalamat [Telebrix Gastro]; Guerbet).

^{18}F-Galacto-RGD PET

Imaging was performed with an ECAT EXACT PET scanner (Siemens). After injection of ^{18}F-galacto-RGD (182.5 ± 38.2 MBq), a transmission scan was acquired for 5 min per bed position (5 bed positions) using 3 rotating ^{68}Ge rod sources (each with approximately 90 MBq ^{68}Ge). A static emission scan in 2-dimensional mode was acquired in the caudocranial direction on each subject, beginning, on average, 58.9 ± 8.4 min after intravenous injection of ^{18}F-galacto-RGD, covering a field of view from the pelvis to the thorax (5–7 bed positions, 8 min per bed position).

Positron emission data were corrected for randoms, dead time, and attenuation and were reconstructed using the ordered-subsets expectation maximization (OSEM) algorithm using 8 iterations and 4 subsets. The images were corrected for attenuation using the collected transmission data. OSEM images underwent a 5-mm full width at half maximum gaussian after smoothing and were zoomed with a factor of 1.2. For image analysis, CAPP software, version 7.1 (Siemens) was used.

^{18}F-FDG PET

Imaging was performed with a Biograph Sensation 16 PET/CT scanner, which incorporates an ACCEL PET camera and a 16-slice multidetector CT (Siemens). Patients were injected with ^{18}F-FDG after 6 h of fasting. None of the patients was diabetic or had a fasting blood glucose level above 120 mg/dL.

Scanning was performed 61.2 ± 3.6 min after intravenous injection of 463.5 ± 20.4 MBq ^{18}F-FDG. A PET scan was performed in the craniocaudal direction covering a field of view from the head to the pelvis (3-dimensional mode; 7 or 8 bed positions, 2 min per bed position). An unenhanced low-dose CT scan was performed for attenuation correction in shallow expiration (120 kV, 26 mAs; collimation, 16 × 0.75 mm) after the PET scan. CT data were converted from Hounsfield units to linear attenuation coefficients for 511 keV using a single CT energy scaling method based on a bilinear transformation. Emission data were corrected for randoms, dead time, scatter, and attenuation, and the same reconstruction algorithm was applied as that used for the conventional PET data. The images were zoomed with a factor of 1.23. For image analysis, the e-soft software was used (Siemens).

Image Analysis

The emission scans were calibrated to standardized uptake values (SUVs). The SUV was calculated according to the following formula: (measured activity concentration [Bq/mL] × body weight [g])/injected activity [Bq]. Up to 5 lesions were chosen in each patient for measurements of SUVs. If there were $>$5 lesions present (n = 4 patients), the lesion with the highest tracer uptake in each afflicted organ system (lung, liver, brain, adrenals, bone, lymph nodes, other) was chosen. The maximum number of 5 lesions per patient was chosen to avoid a bias by patients with an exceptionally high number of lesions. A volume of interest (VOI) was drawn around each lesion, encompassing the whole lesion. The outer border of each lesion VOI was semiautomatically defined by an isocontour representing 60% of the maximum activity within the VOI. The mean SUV in this VOI was used for further analysis. For lesions that were not identifiable on ^{18}F-galacto-RGD PET, the VOI was placed at the site of the metastases according to CT and ^{18}F-FDG PET.

For analysis of sensitivity of ^{18}F-galacto-RGD for lesion identification, the number of lesions in each scan, which were identifiable as either areas of elevated tracer uptake or as photopenic defects in an organ, was noted. The findings of the clinical staging procedures served as the standard of reference (including

TABLE 1
Patient Characteristics

Patient no.	Age (y)	Pathology	Lesion localization	SUV_{mean}	
				^{18}F-Galacto-RGD	^{18}F-FDG
1	55	Renal cell carcinoma	Bone	3.42	4.18
			Bone	1.10	3.39
2	66	Hemangiosarcoma	Primary, liver	1.78	3.67
3	55	Squamous cell carcinoma of head and neck	Primary	2.01	9.81
			Lymph node	2.00	7.88
			Lymph node	1.99	8.52
			Lung	0.30	3.25
4	54	Invasive ductal breast cancer	Primary, breast	3.50	5.16
			Liver	2.50	4.21
			Bone	3.08	1.29
5	70	NSCLC	Primary, lung	3.14	10.94
			Lymph node	3.20	7.25
			Lymph node	3.49	4.87
			Bone	4.66	9.82
			Bone	0.80	6.82
6	62	NSCLC	Primary, lung	2.29	7.66
			Metastasis, lung	0.30	1.74
			Cerebrum	0.63	1.96
7	71	NSCLC	Primary, lung	1.29	9.09
			Metastasis, lung	1.25	5.26
			Lymph node	1.00	2.92
			Adrenal gland	3.03	23.20
			Liver	2.02	3.76
8	62	NSCLC	Primary, lung	4.01	9.65
			Bone	5.80	10.29
			Bone	5.03	6.07
			Intestine	5.23	20.45
			Lymph node	3.15	4.02
9	64	Renal cell carcinoma	Liver	1.66	3.79
			Retroperitoneum	0.30	1.82
10	68	Carcinoid of bronchus	Primary	4.45	2.21
			Liver	6.82	4.55
			Spleen	5.95	3.75
			Lymph node	6.15	7.14
			Bone	5.42	3.21
11	73	NSCLC	Primary, lung	2.45	13.73
			Bone	2.09	10.99
			Liver	1.96	13.94
			Liver	2.21	17.43
			Liver	2.61	18.63
12	71	Adenocarcinoma of rectum	Lung	3.48	8.56
			Lymph node	1.10	5.36
13	52	NSCLC	Primary, lung	3.43	2.86
			Lymph node	3.32	2.29
			Cerebrum	1.22	3.43
14	72	NSCLC	Primary, lung	3.19	9.69
			Bone	2.48	10.29
			Adrenal gland	1.88	11.51
			Liver	2.75	11.61
			Bone	3.00	8.50
15	52	Adenocarcinoma of rectum	Liver	2.34	11.07
16	80	NSCLC	Primary, lung	2.80	7.40
			Liver	1.90	5.10
17	58	NSCLC	Primary, lung	1.49	3.74
			Lymph node	1.83	8.30
			Lymph node	1.83	8.30
18	68	NSCLC	Primary, lung	3.04	18.19
			Lymph node	1.40	4.73
			Lymph node	2.62	8.25

SUV_{mean} = mean standardized uptake value; NSCLC = non–small cell lung cancer.

contrast-enhanced CT and ^{18}F-FDG PET/CT in all cases), as biopsies and histopathology were not available for most of the analyzed metastases. Again, a maximum number of 5 lesions per patient was considered for further analysis to avoid a bias by patients with an exceptionally high number of lesions ($n = 4$). The reports from the Department of Radiology on the CT scans and from the Department of Nuclear Medicine on the ^{18}F-FDG PET/CT scans were used as reference. Moreover, for comparison with the results of the ^{18}F-galacto-RGD PET scans, data were analyzed retrospectively by a board-certified radiologist who had 4 y of experience using PET/CT.

Statistical Analysis

All quantitative data are expressed as mean ± 1 SD. The correlation between quantitative parameters was evaluated by linear regression analysis and by calculation of the Pearson correlation coefficient *R*. Statistical significance was tested by using ANOVA.

Comparison of quantitative parameters was performed using the Wilcoxon test.

All statistical tests were performed at the 5% level of statistical significance, using the StatView program (SAS Institute Inc.) or MedCalc (MedCalc version 6.15.000).

RESULTS

^{18}F-Galacto-RGD PET Data

The mean ^{18}F-galacto-RGD uptake in all lesions ($n = 59$) was 2.7 ± 1.5. For primaries ($n = 14$) it was 2.9 ± 0.9, for osseous metastases ($n = 11$) it was 3.4 ± 1.7, for liver metastases ($n = 10$) it was 2.7 ± 1.5, and for other metastases ($n = 24$) it was 1.9 ± 1.8 (Fig. 1A). There was no statistically significant difference in SUVs between primaries and all metastases ($P = 0.392$). Osseous metastases showed the highest uptake in the group of metastatic lesions, but the difference in uptake was not statistically significant compared with that of other metastases ($P = 0.116$).

^{18}F-FDG PET Data

The mean ^{18}F-FDG uptake in all lesions ($n = 59$) was 7.6 ± 4.9. For primaries ($n = 14$) it was 8.4 ± 3.5, for osseous metastases ($n = 11$) it was 6.8 ± 3.4, for liver metastases ($n = 10$) it was 9.4 ± 5.9, and for other metastases ($n = 24$) it was 8.1 ± 5.8 (Fig. 1B). There was no statistically significant difference in SUVs between primaries and all metastases ($P = 0.521$). Liver metastases showed the highest uptake in the group of metastatic lesions, but the difference in uptake was not statistically significant compared with that of other metastases ($P = 0.199$).

Comparison of ^{18}F-Galacto-RGD PET and ^{18}F-FDG PET Data

The mean SUV for all lesions ($n = 59$) was significantly higher for ^{18}F-FDG PET than that for ^{18}F-galacto-RGD PET ($P < 0.001$). Only 1 patient showed higher SUVs in the tumor lesions with ^{18}F-galacto-RGD PET compared with those of ^{18}F-FDG PET (patient 10, bronchus carcinoid). ^{18}F-Galacto-RGD PET missed 14 lesions (27%) compared with clinical staging, including contrast-enhanced CT and ^{18}F-FDG PET/CT (sensitivity: 76%). Seven of the missed

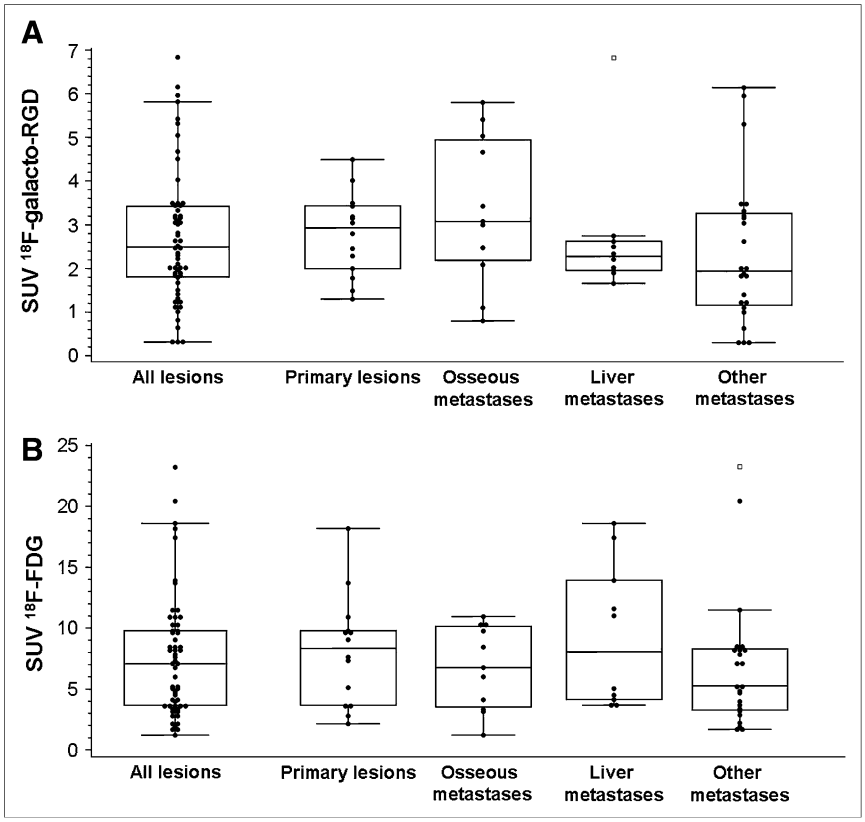

FIGURE 1. Box plot diagram of distribution of SUVs for all lesions and for primary and metastatic lesions separately for ^{18}F-galacto-RGD (A) and ^{18}F-FDG (B). Note significantly higher tracer uptake for ^{18}F-FDG compared with that for ^{18}F-galacto-RGD ($P < 0.0001$).

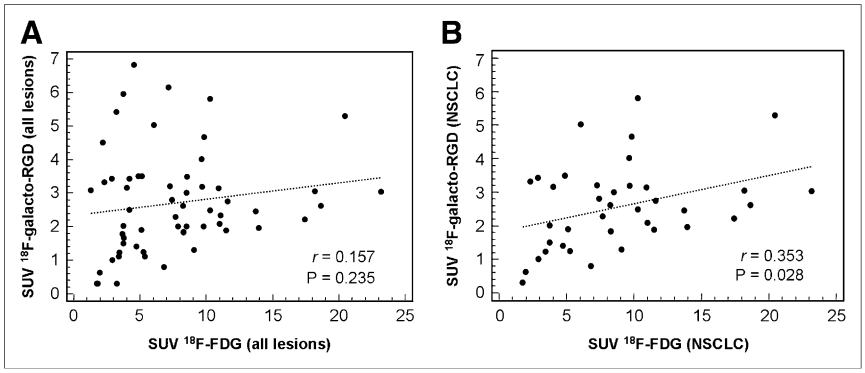

FIGURE 2. Comparison of SUVs from ^{18}F-FDG PET and ^{18}F-galacto-RGD PET for all lesions (A) and for lesions in patients with NSCLC separately (B). No statistically significant correlation is found between uptake of the 2 tracers for all lesions. In the subgroup of lesions in NSCLC, there is a weak correlation between uptake of the 2 tracers—however, with a low correlation coefficient.

lesions were located in the liver, 7 were located in other sites (bone, $n = 2$; lung, $n = 2$; lymph node, $n = 1$; soft tissue, $n = 1$; adrenal gland, $n = 1$).

No significant correlation was found between the SUVs of ^{18}F-galacto-RGD and ^{18}F-FDG PET for all lesions ($r = 0.157$, $P = 0.235$; Fig. 2A). With regard to the separate tumor locations, there was also no significant correlation for primary lesions ($r = -0.068$, $P = 0.817$), osseous metastases ($r = 0.066$, $P = 0.846$), liver metastases ($r = -0.182$, $P = 0.615$), or other metastases ($r = 0.397$, $P = 0.055$). When only the subgroup of ^{18}F-FDG–avid tumors was analyzed (NSCLC, breast cancer, squamous cell carcinoma of head and neck [SCCHN], rectal cancer; $n = 49$), there was a weak correlation between the uptake of the 2 tracers ($r = 0.337$, $P = 0.018$). For the subgroup of lesions in patients with NSCLC ($n = 39$), there was again only a weak correlation ($r = 0.357$; $P = 0.028$; Fig. 2B).

DISCUSSION

In this study we compared the ^{18}F-galacto-RGD uptake and ^{18}F-FDG uptake on PET in primary and metastatic tumor lesions in cancer patients. In general, no substantial correlation between ^{18}F-galacto-RGD and ^{18}F-FDG uptake could be demonstrated, suggesting that $\alpha_v\beta_3$ expression and glucose metabolism are not closely linked in malignant lesions. The sensitivity for lesion detection was significantly higher for ^{18}F-FDG PET compared with that for ^{18}F-galacto-RGD PET. Thus, ^{18}F-FDG PET remains superior for primary staging of cancer patients, whereas ^{18}F-galacto-RGD PET might provide additional information for planning and response evaluation of antiangiogenic therapies.

With regard to all lesions, comparison of the tracer uptake of ^{18}F-FDG and ^{18}F-galacto-RGD showed no correlation between the 2 parameters. This applied to primary lesions as well as to metastatic lesions, independent of the metastatic site. For the subgroup of ^{18}F-FDG–avid lesions and lesions in patients with NSCLC, there was a slight trend toward a higher ^{18}F-galacto-RGD uptake in more ^{18}F-FDG–avid lesions. Notably, lesions with very high ^{18}F-FDG uptake (SUV $>$ 15) all demonstrated at least moderate ^{18}F-galacto-RGD uptake (SUV > 2). However, the correlation coefficient was very low (Fig. 3). As the integrin $\alpha_v\beta_3$ is believed to be a marker of activated endothelial cells, ^{18}F-galacto-RGD is a potential surrogate parameter of angiogenesis in tumors with predominantly endothelial $\alpha_v\beta_3$ expression. Our results suggest that $\alpha_v\beta_3$ expression and glucose metabolism are not closely correlated in tumor lesions and, consequently, ^{18}F-FDG

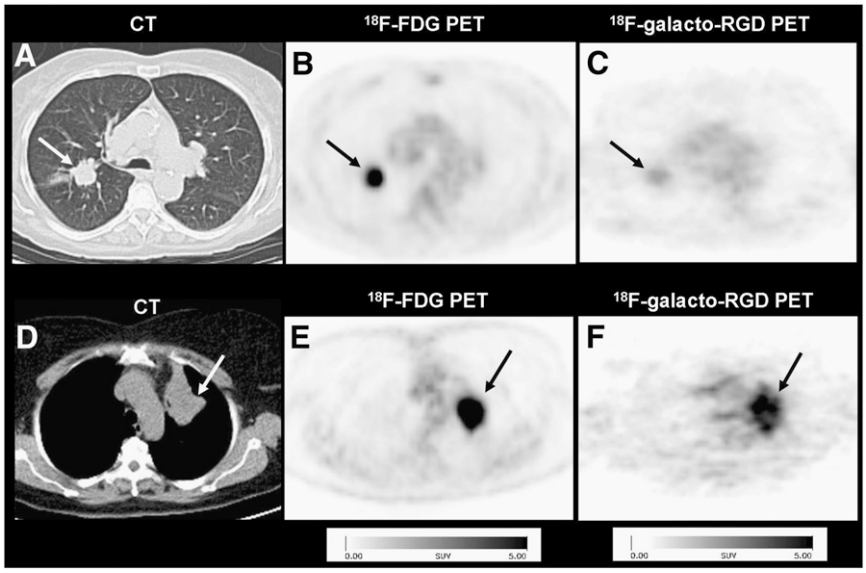

FIGURE 3. Comparison of patients with NSCLC of right lung (A–C) and left lung (D–F; arrows). Note intense uptake in both lesions in ^{18}F-FDG PET (B and E), whereas lesions demonstrate completely different uptake patterns in corresponding ^{18}F-galacto-RGD PET: There is only weak uptake in first patient (C), whereas there is intense uptake in second patient (F).

cannot provide information similar to that of ^{18}F-galacto-RGD. Although these results are not unexpected, reports in the literature describe a correlation between angiogenesis and ^{18}F-FDG uptake in benign and malignant lesions. In human lung adenocarcinomas, which also represented the main patient population in our study, the microvessel density (MVD) of vessels positive for CD105, a proliferation-related endothelial cell marker, correlated positively with ^{18}F-FDG uptake (*16*). Moreover, in human breast cancer, a weak but significant correlation between MVD using CD31 staining and ^{18}F-FDG uptake was demonstrated (*17*). In giant cell tumors, a gene chip analysis showed a close association between ^{18}F-FDG uptake and kinetic ^{18}F-FDG data with the expression of genes related to angiogenesis, such as VEGF A (*9*). As the integrin $\alpha_v\beta_3$ is a key player in angiogenesis as well, a correlation between $\alpha_v\beta_3$ expression and ^{18}F-FDG uptake would have been conceivable according to these results. However, other studies showed no significant correlation between angiogenesis and ^{18}F-FDG uptake, which is more closely in line with our results. In patients with NSCLC, no correlation was found between ^{18}F-FDG uptake and MVD, determined by staining with von Willebrand factor (*18*). In breast cancer patients, one study even showed a slightly negative correlation between ^{18}F-FDG uptake and the density of tumor capillaries (*19*). However, it must be stressed that our results cannot ultimately elucidate the relationship between ^{18}F-FDG uptake and angiogenesis because the exact role of $\alpha_v\beta_3$ expression in the context of angiogenesis is still a matter of debate. Experiments on knockout mice lacking the integrin $\alpha_v\beta_3$ led to a reevaluation of the role of $\alpha_v\beta_3$ with regard to angiogenesis, because the knockout mice showed normal developmental angiogenesis and even excessive tumor angiogenesis (*20*). $\alpha_v\beta_3$ is now assumed to have a positive and a negative regulatory role in angiogenesis depending on the respective biologic context. Moreover, our small number of patients—especially with non–^{18}F-FDG-avid tumors—is a limitation of our study. Therefore, it cannot be excluded that, for certain subgroups of tumors, a closer correlation of ^{18}F-FDG and ^{18}F-galacto-RGD uptake exists.

The tracer uptake of ^{18}F-FDG in tumor lesions was significantly higher than that of ^{18}F-galacto-RGD. This is in accordance with the suggested pharmacodynamics of both tracers, because ^{18}F-FDG accumulates in the tumor cells whereas ^{18}F-galacto-RGD binds predominantly to endothelial cells. As the number of endothelial cells—even in highly vascularized tumors—is substantially smaller than the number of tumor cells, the difference in tracer uptake corroborates the suggested binding mechanisms for both substances (*21*).

Conventional staging, including contrast-enhanced CT and ^{18}F-FDG PET, identified substantially more lesions than ^{18}F-galacto-RGD PET (Fig. 4A). This illustrates that with regard to tumors in which ^{18}F-FDG PET has already demonstrated good results for staging, ^{18}F-galacto-RGD PET is unlikely to produce better results, including NSCLC, breast cancer, and SCCHN (*22–24*). This is not surprising, as the primary intention for the development of this tracer was not to replace ^{18}F-FDG or to improve tumor staging but, rather, to create a tool for molecular imaging of processes related to $\alpha_v\beta_3$ expression, such as angiogenesis. However, in 1 patient with a bronchus carcinoid, tracer uptake on ^{18}F-galacto-RGD PET was substantially higher than that on ^{18}F-FDG PET in the primary tumor as well as in the metastases (Fig. 4B). Therefore, in tumors with low or intermediate ^{18}F-FDG uptake, such as prostate cancer or carcinoid tumors, imaging of $\alpha_v\beta_3$ expression might produce better results for lesion identification and tumor staging than those of ^{18}F-FDG PET (*25,26*). This, however, is only a hypothesis and must be proven in future prospective studies. Moreover, variations in tracer design are undertaken to further improve the performance of $\alpha_v\beta_3$ imaging. This includes, for example, multimeric RGD peptides with >1 RGD binding site per molecule, which have already demonstrated improved tumor uptake and tumor-to-background contrast in vitro and in vivo compared with monomeric RGD peptides (*27–30*). One small-animal PET study in tumor-bearing mice—which compared ^{18}F-FDG and imaging of $\alpha_v\beta_3$ expression with a ^{64}Cu-labeled PEGylated dimeric RGD peptide in a model of lung cancer (NCI-H1975 lung adenocarcinoma)—even showed higher tumor-to-background ratios for the RGD peptide compared with those of ^{18}F-FDG (*31*). Thus, it is conceivable that, in the future, PET of $\alpha_v\beta_3$ expression might prove to be superior to ^{18}F-FDG even in tumors with good ^{18}F-FDG uptake. Again, this hypothesis remains to be proven in future comparative studies.

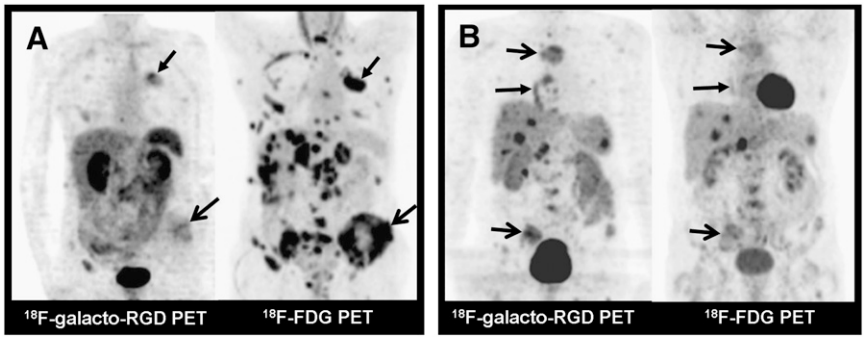

FIGURE 4. Comparison of different uptake patterns in ^{18}F-FDG PET and ^{18}F-galacto-RGD PET. (A) Patient with NSCLC of left upper lobe (arrow, closed tip) and multiple metastases to bone (arrow, open tip), liver, lymph nodes, and adrenal glands. Note intense uptake in all lesions in maximum-intensity-projection (MIP) of ^{18}F-FDG PET, whereas uptake in lesions in MIP of ^{18}F-galacto-RGD PET is substantially lower. This typical uptake pattern is seen in most patients. (B) Patient with neuroendocrine tumor of bronchus in right lower lobe (arrow, closed tip) and multiple metastases to bone (arrows, open tip), liver, spleen, and lymph nodes. This patient shows more intense uptake in lesions on ^{18}F-galacto-RGD PET compared with that on ^{18}F-FDG PET.

Lesion identification in ^{18}F-galacto-RGD PET was particularly difficult in the liver. Seven of 10 liver lesions were undetectable, either as positive or photopenic lesions. Liver lesions were identifiable as a positive lesion in only 1 patient (patient 10, bronchus carcinoid); in 2 patients lesions could be identified indirectly as photopenic defects. Therefore, we conclude that the unsatisfactory detection rate is caused primarily by the relatively high background activity in the liver. This has already been presumed in previous studies on the biodistribution and dosimetry of ^{18}F-galacto-RGD in cancer patients, in whom a comparatively high tracer retention in the liver could be demonstrated (*32,33*). Thus, assessment of $\alpha_v\beta_3$ expression with ^{18}F-galacto-RGD PET in liver lesions with only a moderate or low tracer uptake is problematic. As discussed earlier, this problem might be overcome with a new tracer—for example, with multimeric compounds showing improved target-to-background ratios. On the other hand, osseous metastases showed the highest tracer uptake compared with lesions in other sites, although this trend did not reach statistical significance. One reason for this tendency to a higher ^{18}F-galacto-RGD uptake in osseous metastases could be attributed to $\alpha_v\beta_3$ expression on tumor cells in addition to endothelial cells, as $\alpha_v\beta_3$ expression is a well-known factor for metastatic spread, especially to the bone (*34,35*). Moreover, $\alpha_v\beta_3$ expression on osteoclasts is a well-known phenomenon in processes involving bone resorption, such as osseous metastases, which could also contribute to the ^{18}F-galacto-RGD PET signal (*36*). However, we can only speculate on the reasons for this finding, because we did not perform immunohistochemical studies in our patient population, which is a general limitation of this study. Such studies were not undertaken for ethical reasons. The primary histopathologic diagnosis had already been established by biopsy as an inclusion criterion, and immunohistochemical studies of $\alpha_v\beta_3$ expression would have necessitated additional biopsies to collect fresh frozen tissue samples, which seemed inappropriate to us in a population of patients with metastatic tumors. Moreover, immunohistochemistry can show only parts of the tumor, which might bias the interpretation in case of heterogeneity of $\alpha_v\beta_3$ expression. Furthermore, samples for immunohistochemistry might not necessarily have been taken from a representative area. Molecular imaging, on the other hand, has the potential to show specific biologic properties of tissues as a whole and also in several tumor sites in the body in one session (*37*).

Another limitation is that we did not perform dynamic studies; only static PET scans were acquired so we could undertake a semiquantitative assessment of tracer uptake by calculating SUVs. However, dynamic scanning limits the field of view to one bed position and would have greatly reduced the number of lesions available for analysis compared with static PET scans. Moreover, it had already been demonstrated for ^{18}F-FDG that dynamic PET data and static PET data correlate reasonably well (*38*). For ^{18}F-galacto-RGD PET, a significant correlation of $\alpha_v\beta_3$ expression and SUVs has also been successfully demonstrated (*8*). However, for truly quantitative studies, dynamic scans and kinetic modeling still would need to be performed (*39*).

Finally, scans were acquired on different scanners. However, a highly significant correlation of SUVs from the Sensation Biograph 16 scanner and a stand-alone PET scanner has recently been demonstrated (*40*).

CONCLUSION

Tracer uptake of ^{18}F-galacto-RGD and ^{18}F-FDG does not correlate closely in malignant lesions, suggesting that each tracer provides complementary information in cancer patients. Whereas ^{18}F-FDG PET is superior for tumor staging because of a higher sensitivity in most tumor entities, ^{18}F-galacto-RGD PET warrants further evaluation for planning and response evaluation of targeted molecular therapies with antiangiogenic or $\alpha_v\beta_3$-targeted drugs.

ACKNOWLEDGMENTS

We thank the Cyclotron and PET team—especially Michael Herz, Gitti Dzewas, Coletta Kruschke, and Nicola Henke—for excellent technical assistance and the Münchner Medizinische Wochenschrift and the Sander Foundation for financial support.

REFERENCES

1. Lyseng-Williamson KA, Robinson DM. Spotlight on bevacizumab in advanced colorectal cancer, breast cancer, and non-small cell lung cancer. *BioDrugs.* 2006; 20:193–195.
2. Morabito A, De Maio E, Di Maio M, Normanno N, Perrone F. Tyrosine kinase inhibitors of vascular endothelial growth factor receptors in clinical trials: current status and future directions. *Oncologist.* 2006;11:753–764.
3. Brooks PC, Clark RAF, Cheresh DA. Requirement of vascular integrin $\alpha_v\beta_3$ for angiogenesis. *Science.* 1994;2674:569–571.
4. Beekman KW, Colevas AD, Cooney K, et al. Phase II evaluations of cilengitide in asymptomatic patients with androgen-independent prostate cancer: scientific rationale and study design. *Clin Genitourin Cancer.* 2006;4:299–302.
5. Friess H, Langrehr JM, Oettle H, et al. A randomized multi-center phase II trial of the angiogenesis inhibitor Cilengitide (EMD 121974) and gemcitabine compared with gemcitabine alone in advanced unresectable pancreatic cancer. *BMC Cancer.* 2006;6:285.
6. Haubner R, Wester HJ, Weber WA, et al. Noninvasive imaging of alpha$_v$beta$_3$ integrin expression using ^{18}F-labeled RGD-containing glycopeptide and positron emission tomography. *Cancer Res.* 2001;61:1781–1785.
7. Haubner R, Weber WA, Beer AJ, et al. Non-invasive visualization of the activated $\alpha_v\beta_3$ integrin in cancer patients by positron emission tomography and [^{18}F]galacto-RGD. *PLoS Med.* March 29, 2005 [Epub ahead of print].
8. Beer AJ, Haubner R, Sarbia M, et al. Positron emission tomography using [^{18}F]galacto-RGD identifies the level of integrin alpha$_v$beta$_3$ expression in man. *Clin Cancer Res.* 2006;12:3942–3949.
9. Strauss LG, Dimitrakopoulou-Strauss A, Koczan D, et al. ^{18}F-FDG kinetics and gene expression in giant cell tumors. *J Nucl Med.* 2004;45:1528–1535.
10. Pedersen MW, Holm S, Lund EL, Hojgaard L, Kristjansen PE. Coregulation of glucose uptake and vascular endothelial growth factor (VEGF) in two small-cell lung cancer (SCLC) sublines in vivo and in vitro. *Neoplasia.* 2001;3:80–87.
11. Gasparini G, Brooks PC, Biganzoli E, et al. Vascular integrin alpha$_v$beta$_3$: a new prognostic indicator in breast cancer. *Clin Cancer Res.* 1998;4:2625–2634.
12. Zhang ZJ, Chen JH, Meng L, et al. ^{18}F-FDG uptake as a biologic factor predicting outcome in patients with resected non-small-cell lung cancer. *Chin Med J (Engl).* 2007;120:125–131.
13. Higashi K, Ito K, Hiramatsu Y, et al. ^{18}F-FDG uptake by primary tumor as a predictor of intratumoral lymphatic vessel invasion and lymph node involvement in

non-small cell lung cancer: analysis of a multicenter study. *J Nucl Med.* 2005;46: 267–273.
14. Lee JD, Yun M, Lee JM, et al. Analysis of gene expression profiles of hepatocellular carcinomas with regard to ^{18}F-fluorodeoxyglucose uptake pattern on positron emission tomography. *Eur J Nucl Med Mol Imaging.* 2004;31:1621–1630.
15. Haubner R, Kuhnast B, Mang C, et al. [^{18}F]Galacto-RGD: synthesis, radiolabeling, metabolic stability, and radiation dose estimates. *Bioconjug Chem.* 2004;15:61–69.
16. Guo J, Higashi K, Ueda Y, et al. Microvessel density: correlation with ^{18}F-FDG uptake and prognostic impact in lung adenocarcinomas. *J Nucl Med.* 2006;47: 419–425.
17. Bos R, van Der Hoeven JJ, van Der Wall E, et al. Biologic correlates of ^{18}fluorodeoxyglucose uptake in human breast cancer measured by positron emission tomography. *J Clin Oncol.* 2002;15:379–387.
18. Cherk MH, Foo SS, Poon AM, et al. Lack of correlation of hypoxic cell fraction and angiogenesis with glucose metabolic rate in non-small cell lung cancer assessed by ^{18}F-fluoromisonidazole and ^{18}F-FDG PET. *J Nucl Med.* 2006;47: 1921–1926.
19. Avril N, Menzel M, Dose J, et al. Glucose metabolism of breast cancer assessed by ^{18}F-FDG PET: histologic and immunohistochemical tissue analysis. *J Nucl Med.* 2001;42:9–16.
20. Hynes RO. A reevaluation of integrins as regulators of angiogenesis. *Nat Med.* 2002;8:918–921.
21. Vermeulen PB, Roland L, Mertens V, et al. Correlation of intratumoral microvessel density and p53 protein overexpression in human colorectal adenocarcinoma. *Microvasc Res.* 1996;51:164–174.
22. Vansteenkiste JF, Stroobants SS. PET scan in lung cancer: current recommendations and innovation. *J Thorac Oncol.* 2006;1:71–73.
23. Mankoff DA, Eubank WB. Current and future use of positron emission tomography (PET) in breast cancer. *J Mammary Gland Biol Neoplasia.* 2006;11:125–136.
24. Koshy M, Paulino AC, Howell R, et al. F-18 FDG PET-CT fusion in radiotherapy treatment planning for head and neck cancer. *Head Neck.* 2005;27:494–502.
25. Kruger S, Buck AK, Blumstein NM, et al. Use of integrated FDG PET/CT imaging in pulmonary carcinoid tumours. *J Intern Med.* 2006;260:545–550.
26. Powles T, Murray I, Brock C, et al. Molecular positron emission tomography and PET/CT I maging in urological malignancies. *Eur Urol.* January 23, 2007 [Epub ahead of print-.
27. Janssen MLH, Oyen WJG, Massuger LFAG, et al. Comparison of a monomeric and dimeric radiolabeled RGD-peptide for tumor imaging. *Cancer Biother Radiopharm.* 2002;17:641–646.
28. Thumshirn G, Hersel U, Goodman SL, et al. Multimeric cyclic RGD peptides as potential tools for tumor targeting: solid-phase peptide synthesis and chemoselective oxime ligation. *Chemistry.* 2003;9:2717–2725.
29. Dijkgraaf I, Kruijtzer JA, Liu S, et al. Improved targeting of the alpha$_v$beta$_3$ integrin by multimerisation of RGD peptides. *Eur J Nucl Med Mol Imaging.* 2007; 34:267–273.
30. Poethko T, Schottelius M, Thumshirn G, et al. Chemoselective pre-conjugate radiohalogenation of unprotected mono- and multimeric peptides via oxime formation. *Radiochim Acta.* 2004;92:317–327.
31. Chen X, Sievers E, Hou Y, et al. Integrin alpha v beta 3-targeted imaging of lung cancer. *Neoplasia.* 2005;7:271–279.
32. Beer AJ, Haubner R, Goebel M, et al. Biodistribution and pharmacokinetics of the $\alpha_v\beta_3$-selective tracer ^{18}F-galacto-RGD in cancer patients. *J Nucl Med.* 2005; 46:1333–1341.
33. Beer AJ, Haubner R, Wolf I, et al. PET-based human dosimetry of ^{18}F-galacto-RGD, a new radiotracer for imaging $\alpha_v\beta_3$ expression. *J Nucl Med.* 2006;47:763–769.
34. Sloan EK, Pouliot N, Stanley KL, et al. Tumor-specific expression of $\alpha_v\beta_3$ integrin promotes spontaneous metastasis of breast cancer to bone. *Breast Cancer Res.* April 11, 2006 [Epub ahead of print].
35. Liapis H, Flath A, Kitazawa S. Integrin alpha v beta 3 expression by bone-residing breast cancer metastases. *Diagn Mol Pathol.* 1996;5:127–135.
36. Nakamura I, Pilkington MF, Lakkakorpi PT, et al. Role of alpha$_v$beta$_3$ integrin in osteoclast migration and formation of the sealing zone. *J Cell Sci.* 1999;112: 3985–3993.
37. Weber WA. Positron emission tomography as an imaging biomarker. *J Clin Oncol.* 2006;24:3282–3292.
38. Weber WA, Schwaiger M, Avril N. Quantitative assessment of tumor metabolism using FDG-PET imaging. *Nucl Med Biol.* 2000;27:683–687.
39. Krohn KA, Mankoff DA, Muzi M, et al. True tracers: comparing FDG with glucose and FLT with thymidine. *Nucl Med Biol.* 2005;32:663–671.
40. Souvatzoglou M, Ziegler SI, Martinez MJ, et al. Standardised uptake values from PET/CT images: comparison with conventional attenuation-corrected PET. *Eur J Nucl Med Mol Imaging.* 2007;34:405–412.